Highly directional acoustic waves generated by a horned parametric acoustic array loudspeaker

L.H. Tong[1], S.K. Lai[2,*], J.W. Yan[3], C. Li[4]

[1] School of Civil Engineering and Architecture, East China Jiaotong University, Nanchang, Jiangxi, P.R. China

[2] Department of Civil and Environmental Engineering, The Hong Kong Polytechnic University, Hung Hom, Kowloon, Hong Kong, P.R. China

[3] Key Laboratory of Product Packaging and Logistics of Guangdong Higher Education Institutes, Jinan University, Zhuhai, Guangdong, P.R. China

[4] School of Urban Rail Transportation, Soochow University, Suzhou, Jiangsu, P.R. China

ABSTRACT

Acoustic horns can enhance the overall efficiency of loudspeakers to emanate highly directional acoustic waves. In this work, a theoretical model is developed to predict difference frequency acoustic fields generated by a parametric array loudspeaker with a flared horn. Based on this model, analytical solutions are obtained for exponentially horned parametric array loudspeakers. A numerical analysis on the performance of horned parametric array loudspeakers subject to various horn parameters (i.e., horn length and flare constant) is implemented. To compare with non-horned parametric acoustic array devices, it is able to generate highly directional acoustic wave beams for a wide range of difference frequencies, in which the generated sound pressure levels at low frequencies can

*Corresponding author. E-mail: sk.lai@polyu.edu.hk (S.K. Lai)

be significantly enhanced. In addition, the equivalent radius of a non-horned emitter that matches the directivity achieved by a horned one is also quantitatively investigated. The present research will provide useful guidelines for the design and optimization of horned parametric array equipment.

Keywords: Parametric acoustic array, Highly directional acoustic waves, Horn length, Flare constant

1. Introduction

Directional acoustic sources can be found in a variety of engineering fields and applications. Several methods have been proposed to pursue highly directional acoustic beams. The pioneering work can be traced back to the parametric acoustic array (PAA) that was made of two collimated acoustic beams in air [1]. The collimated acoustic beams in a high-frequency range are called as the primary frequency beam. Both high-frequency sum components and low-frequency difference components can be generated by the nonlinear interaction of primary acoustic beams. The high-frequency components are quickly absorbed by air, and thus only the low-frequency components can continually propagate outward.

In general, there are two approaches to generate highly directional acoustic beams. Westervelt [1] firstly theoretically predicted a highly directional acoustic beam that can be created by the low-frequency components. Secondly, a two-dimensional phononic crystal resonant cavity, having a point acoustic source located inside, can be served another highly directional acoustic device [2-5]. To compare with PAA devices, the latter one is mainly used to generate highly directive ultrasonic waves rather than audible sound waves, thus it is not applicable for daily life situations.

Since the discovery of PAA devices, many research studies have dedicated to this topic in terms of theoretical analysis and experimental studies [6-14]. In particular, the convolution model proposed by Shi and Kajikawa [6] is an effective method to compute the far-field directivity of PAA devices with negligible computational cost. Due to the prominent characteristics of PAA devices (e.g., high directivity effect), many potential applications are able to be truly realized. For instance, a parametric array loudspeaker (PAL)

is a typical application of PAA devices [14]. With the advancement of pre-processing techniques [7], the effect of nonlinear distortion can be greatly reduced, thereby improving the quality of PAA devices. Inspired by the discovery of PAL, other important applications, i.e., active noise control and omni-directional sound pressure field generation, have been proposed from the high directivity of PAA devices [15, 16]. Although we have witnessed the innovative development of PAA devices to improve audio quality and speech experience, a daunting technical challenge on the low conversion efficiency, especially within a low-frequency range, still remains unsolved.

Unlike conventional loudspeakers, PAA devices are able to generate highly directional difference acoustic fields within a low-frequency range [17]. To improve the conversion efficiency of PAA devices, Sayin and Guasch [18] assembled an ultra-megaphone with a parametric loudspeaker and a horn. On one hand, the ultra-megaphone can overcome the cut-off problem that exists in conventional exponential horn loudspeakers. On the other hand, the horn can increase the radiation efficiency to improve the conversion efficiency of PAA devices. Previous experimental studies have reported that a horn can make a significant impact on the audible sound level and directivity of parametric loudspeakers [18]. Nevertheless, the intrinsic mechanism of a horn acting on parametric loudspeakers is still absent, this strongly motivates us to establish a universal model to achieve a better understanding of the working principle.

In this paper, a theoretical model is proposed for horned PAA devices. On the basis of this model, analytical solutions can be obtained for exponentially horned parametric array loudspeakers. The performance of horned parametric array loudspeakers is investigated by a numerical analysis. This is different from non-horned parametric acoustic array devices,

it is able to generate highly directional acoustic wave beams for a wide range of difference frequencies. From the obtained results, the secondary acoustic pressure can be considerably increased at low frequencies. To improve the directivity of a horned PAL over a non-horned PAL, the radius ratio of both horned and non-horned emitters is also studied. The present work will facilitate a design approach for the optimization of horned parametric acoustic array loudspeakers in real engineering applications.

2. Mathematical Formulation and Solutions

A schematic diagram for the geometry of a horned parametric acoustic array loudspeaker is presented in Fig. 1(a). The primary source of this horned parametric acoustic array loudspeaker is composed of an array of piezoelectric transducers as illustrated. We take a volume element of length dx and area $S(x)$ at x within the horn as shown in Figs. 1(b) and 1(c). Besides, a typical circuit to drive the parametric array is also presented in Fig. 1(d). Two original signals are generated by a signal generator and then they are fed into amplifiers after being synchronized. The final amplified signals are directly applied on the parametric array. The purpose of the signal synchronization is to guarantee that all the output ultrasound signals have no phase difference to avoid the interference of the primary waves. The components shown in the dotted frame of Fig. 1(d) indicate the special processing arrangement for the directional emission of wideband signals. The detailed information for the signal processing can be referred to Ref. [11]. In this work, we only consider the geometrical configuration of a horn, because the major focus is to investigate the influence of this horn on the performance of parametric acoustic array loudspeakers.

Let u be a particle velocity parallel to the horn axis x. The mass variation in the volume element per unit time is $-\frac{\partial}{\partial x}\left[\rho u S\left(x\right)dx\right]$ with ρ being the density of a medium in which acoustic waves propagate. As the volume element is small, its mass is approximately equal to $\rho S\left(x\right)dx$ and the corresponding mass variation rate is $\frac{\partial}{\partial t}\left[\rho S(x)dx\right]$. According to the law of conservation of mass, the continuity equation is given by

$$\frac{\partial\left(\rho S\right)}{\partial t}+\frac{\partial\left(\rho u S\right)}{\partial x}=0 \tag{1}$$

Suppose that the propagating acoustic wave is a plane wave, then the area of the wavefront can be regarded as the cross-sectional area $S(x)$ of the horn. By ignoring the viscosity of the surrounding medium, the equation of motion is then expressed as [19]

$$\frac{\partial u}{\partial t}+u\frac{\partial u}{\partial x}=-\frac{1}{\rho}\frac{\partial P}{\partial x} \tag{2}$$

where P is the acoustic pressure in the surrounding medium. Multiplying Eq. (1) by u and then adding to Eq. (2) yield

$$\frac{\partial\left(\rho u\right)}{\partial t}+\frac{\partial\left(\rho u^{2}\right)}{\partial x}=-\frac{\partial P}{\partial x}-\rho u^{2}\frac{d\left(\ln S\right)}{dx} \tag{3}$$

Adding the term $C_0^{\,2}\left(\partial\rho/\partial x\right)$ to both sides of Eq. (3), we have

$$\frac{\partial\left(\rho u\right)}{\partial t}+C_0^{\,2}\frac{\partial\rho}{\partial x}=-\frac{\partial T_x}{\partial x}-\rho u^{2}\frac{d\left(\ln S\right)}{dx} \tag{4}$$

where $T_x=P+\rho u^2-\rho C_0^{\,2}$ with C_0 being the isentropic wave velocity in the surrounding medium. Taking the derivatives of Eqs. (1) and (4) with respect to t and x, respectively, then subtracting these two equations, the wave equation for the acoustic pressure P is obtained as

$$\frac{\partial^2 P}{\partial x^2}-\frac{1}{C_0^{\,2}}\frac{\partial^2 P}{\partial t^2}=\frac{1}{C_0^{\,2}}\frac{\partial^2\left(\rho C_0^{\,2}-P\right)}{\partial t^2}-\frac{\partial^2\left(\rho u^2\right)}{\partial x^2}-\frac{\partial}{\partial x}\left(\rho u^2\frac{d\ln S}{dx}\right)+\frac{d\ln S}{dx}\frac{\partial\left(\rho u\right)}{\partial t} \quad (5)$$

The inhomogeneous terms on the right-hand side of Eq. (5) are very complicated, thus some simplifications should be made. Take the second-order approximation of $\rho-\left(P/C_0^{\,2}\right)$ to result in [20]

$$\rho-\frac{P}{C_0^{\,2}}=\rho-\frac{1}{C_0^{\,2}}\left[P_0+\left(\frac{\partial P}{\partial\rho}\right)_{\rho=\rho_0}\left(\rho-\rho_0\right)+\frac{1}{2}\left(\frac{\partial^2 P}{\partial\rho^2}\right)_{\rho=\rho_0}\left(\rho-\rho_0\right)^2\right] \quad (6)$$

where P_0 is a static pressure. Consider $\left(\partial P/\partial\rho\right)_{\rho=\rho_0}=C_0^{\,2}$, $P_0=\rho_0 C_0^{\,2}$ and $P-P_0=\left(\rho-\rho_0\right)C_0^{\,2}$, Eq. (6) is further simplified as

$$\rho-\frac{P}{C_0^{\,2}}=\rho_0-\frac{P_0}{C_0^{\,2}}-\frac{1}{2}\frac{p^2}{C_0^{\,6}}\left(\frac{\partial^2 P}{\partial\rho^2}\right)_{\rho=\rho_0} \quad (7)$$

where $p=P-P_0$ is the variation of the acoustic pressure. Expanding the third inhomogeneous term, we have

$$\frac{\partial}{\partial x}\left(\rho u^2\frac{d\ln S}{dx}\right)=\frac{d\ln S}{dx}\frac{\partial\left(\rho u^2\right)}{\partial x}+\rho u^2\frac{d^2\left(\ln S\right)}{dx^2} \quad (8)$$

Given that the cross-sectional area of the horn changes slowly and ρu^2 is a second-order small quantity, thus the second term on the right-hand side of Eq. (8) can be neglected with no significant error. If an exponential horn is considered, then the second term on the right-hand side is equal to zero. For the other two inhomogeneous terms, we apply a linear approximation on them and combine Eqs. (7) and (8) together, then Eq. (5) is simplified as

$$\frac{\partial^2 p}{\partial x^2}+\frac{d\ln S}{dx}\frac{\partial p}{\partial x}-\frac{1}{C_0{}^2}\frac{\partial^2 p}{\partial t^2}=-\frac{1}{2}\frac{1}{C_0{}^6}\left(\frac{\partial^2 P}{\partial \rho^2}\right)_{\rho=\rho_0}\frac{\partial^2 p^2}{\partial t^2}-\rho_0\frac{\partial^2 u^2}{\partial x^2}-\rho_0\frac{d\ln S}{dx}\frac{\partial u^2}{\partial x} \quad (9)$$

If the second-order quantities u^2 and p^2 in Eq. (9) are neglected, then the pressure p can be recovered to a linear acoustic pressure field p_1. Therefore, the linear acoustic pressure p_1 satisfies the following homogeneous equation

$$\frac{\partial^2 p_1}{\partial x^2}+\frac{d\ln S}{dx}\frac{\partial p_1}{\partial x}-\frac{1}{C_0{}^2}\frac{\partial^2 p_1}{\partial t^2}=0 \quad (10)$$

According to Westervelt's parametric array theory [1], the sum or difference acoustic pressure levels can be resulted from the interaction of the first-order acoustic pressure fields. Hence, p_1 is viewed as a source of the sum or difference acoustic pressure fields. Because of the high attenuation of the sum acoustic pressure field, only the difference acoustic field p_s is investigated here. The difference acoustic pressure field satisfies the following equation

$$\nabla^2 p_s-\frac{1}{C_0{}^2}\frac{\partial^2 p_s}{\partial t^2}=-\frac{1}{2}\frac{1}{C_0{}^6}\left(\frac{\partial^2 P}{\partial \rho^2}\right)_{\rho=\rho_0}\frac{\partial^2 p_1{}^2}{\partial t^2}-\rho_0\frac{\partial^2 u^2}{\partial x^2}-\rho_0\frac{d\ln S}{dx}\frac{\partial u^2}{\partial x} \quad (11)$$

where ∇^2 is the Laplace operator. Making use of the first-order approximation of the particle velocity u, then p_1 and u can comply with a linear relation $p_1=uZ_a$, where Z_a is a specific wave impedance of the horn. Consider $\nabla^2 p_1{}^2=\Box^2 p_1{}^2+C_0^{-2}\left(\partial^2/\partial t^2\right)p_1{}^2$ along with the fact that $\Box^2 p_1{}^2$ does not have contribution to p_s [1], where $\Box^2$ is the d'Alembert operator, Eq. (11) can be re-written as

$$\nabla^2 p_s - \frac{1}{C_0^{\,2}}\frac{\partial^2 p_s}{\partial t^2} = -\rho_0 \frac{\partial q}{\partial t} - \frac{\rho_0}{Z_a^{\,2}}\frac{d\ln S}{dx}\frac{\partial p_1^{\,2}}{\partial x} \tag{12}$$

where $q = \dfrac{1}{\left(\rho_0 C_0^{\,2}\right)^2}\left(\beta + \dfrac{\rho_0^{\,2} C_0^{\,2}}{Z_a^{\,2}} - 1\right)\dfrac{\partial p_1^{\,2}}{\partial t}$ with $\beta = \dfrac{1}{2}\dfrac{\rho_0}{C_0^{\,2}}\left(\dfrac{\partial^2 P}{\partial \rho^2}\right)_{\rho=\rho_0} + 1$ being a nonlinear coefficient. Equations (10) and (12) are the governing equations of the difference frequency waves. When *S* is a constant, the governing equations are the same as the results presented by Westervelt [1].

If the horn length is infinitely long, no reflected waves exist in the solution of Eq. (10). For simplicity, the exponential horn that is characterized by a cross-sectional area $S(x) = S_0 \exp(\delta x)$ is investigated here, in which S_0 is the cross-sectional area at the throat of the horn and δ is the flare constant. Assume that the circular frequency of the primary wave is ω, Eq. (10) can be solved as $p_1(x,t) = A\exp(-\delta x/2)\exp\left[j(\omega t - \kappa x)\right]$ with $\kappa = \sqrt{(\omega/C_0)^2 - (\delta/2)^2}$ [19]. For a finite-length horn, it is easily verified that the amplitude of the reflected wave is greatly small as compared with that of the incident wave. Hence, $ka_L > 3$ can be ignored, where a_L is the radius of the cross-section at the mouth of the horn [19]. For a high-frequency primary wave, the solution to Eq. (10) for a finite-length horn is approximately equal to that of an infinite-length one. As the primary wave is always selected in a high-frequency range in this study, we do not differentiate the solution to Eq. (10) for both finite- and infinite-length horns. Let the amplitude of the primary acoustic wave be p_a, the solution to Eq. (10) is [19]

$$p_1(x,t) = p_a e^{-\frac{\delta}{2}x} e^{j(\omega t - \kappa x)} \tag{13}$$

Note that the acoustic wave attenuation is neglected in Eq. (13), so it is only suitable for the acoustic wave in a low-frequency range. As the primary frequency studied here is located in a high-frequency range, the wave attenuation cannot be ignored. Assume that two collimated primary waves, having the circular frequencies (ω_1 and ω_2) and the same pressure amplitude p_a , propagate along the horn. The circular frequencies satisfy $\left|\omega_1-\omega_2\right|<<\omega_1\approx\omega_2$. Let the attenuation coefficient for both waves be α_0, the first-order acoustic field is corrected to

$$p_1\left(x,t\right)=p_a e^{-\frac{\delta}{2}x}e^{-\alpha_0 x}\left[e^{j(\omega_1 t-\kappa_1 x)}+e^{j(\omega_2 t-\kappa_2 x)}\right] \tag{14}$$

where $\kappa_i=\sqrt{\left(\omega_i/C_0\right)^2-\left(\delta/2\right)^2}$, $\left(i=1,2\right)$. It is found that the waves with $2\omega_i$ and $\left|\omega_1\pm\omega_2\right|$ appear in $p_1^{\,2}\left(x,t\right)$. Consider the waves at high frequencies can attenuate sharply, only the difference frequency wave is retained, i.e., $p_1^{\,2}\left(x,t\right)=p_a^{\,2}e^{-\delta x}e^{-2\alpha_0 x}e^{j(\omega_d t-\kappa_d x)}$ where $\omega_d=\left|\omega_1-\omega_2\right|$ and $\kappa_d=\left|\kappa_1-\kappa_2\right|$. The primary wave frequency satisfies $\omega_i/C_0>>\delta/2$, then $\kappa_i\approx\omega_i/C_0=k_i$ $\left(i=1,2\right)$. Substitute the expression of $p_1^{\,2}$ into Eq. (12), the difference frequency acoustic pressure at the observation point P generated by the virtual array on *S*(*x*) in Fig. 1(c) can be obtained by using the Green function method [21] as follows

$$dp_s=-\frac{Qp_a^{\,2}}{4\pi}e^{j\omega_d t}\iint_{S(x)}\left[\frac{e^{-jk_d\mathbf{h}}}{\left|\mathbf{h}\right|}e^{-\left(\delta+2\alpha_0+jk_d\right)x}dx\right]dS \tag{15}$$

where $\mathbf{h}$ is the vector from the area element to the observation point in Fig. 1(c), and $Q=\left[\beta-1+\left(\rho_0C_0/Z_a\right)^2\right]\omega_d^{\,2}/\left(\rho_0C_0^{\,4}\right)+\left(\rho_0/Z_a^{\,2}\right)\delta\left(jk_d+\delta+2\alpha_0\right)$ is the source factor

within a high-frequency range. When $Z_a \approx \rho_0 C_0$ [19], then Q can be simplified as $Q = \left[\beta k_d^{\,2} + \delta\left(jk_d + \delta + 2\alpha_0\right)\right] \Big/ \left(\rho_0 C_0^{\,2}\right)$. It is difficult to obtain explicit solutions to Eq. (15) in the near-field. For the sake of simplification and practicability, the difference frequency acoustic pressure in the far-field is given by [19]

$$\begin{aligned} dp_s &= -\frac{Q p_a^{\,2} S(x)}{4\pi |\mathbf{r}|} e^{j(\omega_d t - k_d \mathbf{r})} e^{-(\delta + 2\alpha_0 + jk_d)x} D(\theta)\, dx \\ &= -\frac{Q p_a^{\,2} S_0}{4\pi |\mathbf{r}|} e^{j(\omega_d t - k_d \mathbf{r})} e^{-(2\alpha_0 + jk_d)x} D(\theta)\, dx \end{aligned} \tag{16}$$

where $\mathbf{r}$ is the vector from the center of the cross section at x to the observation point P, θ is the angle from the axis x to the vector $\mathbf{r}$ (see Fig. 1(c)), $D(\theta) = 2\mathrm{J}_1\left(k_d a_x \sin\theta\right) \big/ \left(k_d a_x \sin\theta\right)$ is the directivity factor of the circular piston, $a_x = a_0 \mathrm{Exp}\left(\delta x/2\right)$ is the radius of the cross section at x, and $\mathrm{J}_1(\cdot)$ is the first-order Bessel function. In the far-field, the approximations $|\mathbf{r}| \approx R_0 - x\cos\nu$ and $\sin\theta \approx \left(R_0 \sin\nu\right) \big/ \left(R_0 - x\cos\nu\right)$ are satisfied, where R_0 is the distance from the center of the horn throat to the observation point, $\nu = \theta\big|_{x=0}$. Based on this, Eq. (16) is approximately equal to

$$dp_s \approx -\frac{Q p_a^{\,2} S_0}{4\pi} e^{j(\omega_d t - k_d R_0)} \frac{e^{-j(k_d - k_d \cos\nu - j2\alpha_0)x}}{R_0 - x\cos\nu} \frac{2\mathrm{J}_1\left(k_d a_x \sin\theta\right)}{k_d a_x \sin\theta} dx \tag{17}$$

The length of the virtual array L_2 satisfies the condition $L_2 >> 1/\left(2\alpha_0\right)$, it is commonly larger than the horn length (see Fig. 1(a)). As a result, the total difference frequency acoustic field in the far-field contains two parts. One is originated from the

virtual array in the horn and the other one is generated outside of the horn. These two effects are given by

$$p_{s1}\left(R_0,\theta,t\right)=-\frac{Qp_a{}^2S_0}{4\pi}e^{j(\omega_d t-k_d R_0)}\int_0^{L_1}\frac{e^{-j(k_d-k_d\cos\nu-j2\alpha_0)x}}{R_0-x\cos\nu}\frac{2\mathrm{J}_1\left(k_d a_x\sin\theta\right)}{k_d a_x\sin\theta}dx \tag{18}$$

and

$$p_{s2}\left(R_0,\theta,t\right)=-\frac{Q'p_a{}^2S_0}{4\pi}e^{j(\omega_d t-k_d R_0)}D\left(\theta_L\right)\int_{L_1}^{L_2}\frac{e^{-j(k_d-k_d\cos\nu-j2\alpha_0)x}}{R_0-x\cos\nu}dx \tag{19}$$

respectively. In Eq. (19), we have $\theta_L=\theta\big|_{x=L_1}$ and $Q'=\left(\beta k_d{}^2\right)\big/\left(\rho_0 C_0{}^2\right)$. The total difference frequency acoustic field can be calculated by the summation of $p_{s1}\left(R_0,\theta,t\right)$ and $p_{s2}\left(R_0,\theta,t\right)$ as

$$p_s\left(R_0,\theta,t\right)=p_{s1}\left(R_0,\theta,t\right)+p_{s2}\left(R_0,\theta,t\right) \tag{20}$$

Within the integration domain (L_1, L_2), the approximation relation $R_0-x\cos\nu\approx R_0$ is well satisfied. Then, the difference frequency acoustic field $p_{s2}\left(R_0,\theta,t\right)$ can be approximately obtained as

$$p_{s2}\left(R_0,\theta,t\right)\approx\frac{Q'p_a{}^2S_0}{8\pi R_0}e^{j(\omega_d t-k_d R_0)}\frac{e^{-j(k_d-k_d\cos\nu-j2\alpha_0)L_2}-e^{-j(k_d-k_d\cos\nu-j2\alpha_0)L_1}}{jk_d\left(\sin\dfrac{\nu}{2}\right)^2+\alpha_0}D\left(\theta_L\right) \tag{21}$$

As the integration of Eq.(18) cannot be solved explicitly, a numerical integration method is employed to obtain the difference frequency acoustic field contributed by the virtual array in the horn. In the subsequent analysis, the numerical integration is directly implemented using the built-in function "*NIntegrate*" in *Mathematica*.

3. Results and Discussion

It is obvious that the difference frequency acoustic fields are significantly affected by the horn flare constant δ as shown in Eqs. (18) and (19). In order to study the characteristics of the difference frequency acoustic fields generated by a horned PAL, a horn with $L_1 = 0.5$ m and $a_0 = 0.1$ m attached to a PAL is taken as an example. The density and the isentropic wave velocity in air are taken as $\rho_0 = 1.29\ \text{kg m}^{-3}$ and $C_0 = 340\ \text{m s}^{-1}$, respectively. The primary wave frequency is selected around 40 kHz and the corresponding attenuation coefficient is $\alpha_0 = 0.2\ \text{m}^{-1}$. From Fig. 2 to Fig. 4, the same parameters are chosen for analysis. The directivity effect of the horned PAL with various flare constants $\delta = 1$, $\delta = 5$ and $\delta = 7$ is presented in Figs. 2(b) - 2(d), respectively. Besides, the directivity for a non-horned case is also shown in Fig. 2 (a) for comparison. The pressure levels in all these figures are normalized to the maximum on-axis pressure. Increasing the flare constant gives rise to a remarkable improvement on the sound directivity and makes the acquired sound beam narrower. By comparing Figs. 2(a) and 2(d), it is found that the sound beam emitted from the non-horned PAL is concentrated within a divergence angle of $\pm 15^{\circ}$. While for the horned PAL with $\delta = 7$, the sound beam almost entirely focuses on the center axis. This is coincident with the available experimental results [18]. In short, a horned PAL is able to emit a much narrower sound beam as compared with a non-horned PAL in both theoretical and experimental studies [11].

In Figs. 2(c) and 2(d), some side lobes are also observed. Using Eq. (21), it is found that the directivity of the difference acoustic field is a coherent result of the two terms, i.e., $1\Big/\left[jk_d \left(\sin\frac{\nu}{2} \right)^2 + \alpha_0 \right]$ and $D(\theta_L)$. Consider the attenuation coefficient α_0 and the

difference wave number k_d, the directivity of the first directive term is independent of the radius of the horn cross section a_x. However, the directivity of the second directive term $D(\theta_L)$ is dependent on $a_x\big|_{x=L_1}$. For a given L_1, $a_x\big|_{x=L_1}$ increases as the flare constant δ increases. It is well known that the side lobes appear in $D(\theta_L)$ for the emitters with a large radius. Therefore, the side lobes appear when the flare constant δ exceeds certain values for the horned PAL as shown in Figs. 2(c) and 2(d). However, for a small flare constant δ, no side lobes appear in Fig. 2(b). It should be pointed out that the amplitudes of the side lobes are greatly smaller than the principal maximum on the center axis, and they do not have influence on the difference frequency acoustic fields.

The output difference frequency acoustic pressure levels under various flare constants are depicted in Fig. 3. It is clearly shown that the acoustic pressure can be remarkably enhanced by increasing the flare constant in the low-frequency difference frequency range (typically less than 1000 Hz). However, the acoustic pressure levels generated by the horned PAL and the non-horned PAL tend to have no difference in the high-frequency range. Therefore, the influence of a horn on the emitted acoustic pressure is mainly within the low-frequency range. This can also be numerically verified by analyzing the source factor Q. In the low-frequency range (typically hundreds of Hz), k_d and δ are on the same order, it implies that the value of the first term may be even smaller than that of the second term in the source factor Q. For the non-horned PAL ($\delta = 0$), the value of the second term in Q vanishes, thus only the first term can make contribution to the acoustic pressure. Increasing the flare constant δ, the value of the second term in Q also increases, this makes more influence on the acoustic pressure. When the difference

frequency increases, i.e., $k_d >> \delta$, the value of the first term in Q is greatly larger than that of the second term, and thus the horn effect on the difference acoustic pressure is weakened.

To further investigate the directivity effect of the horned PAL, the acoustic pressure responses at various difference frequencies are shown in Fig. 4 and the corresponding responses for the non-horned case are also presented. Obviously, the sound pressure levels can be greatly enhanced within the low-frequency range, this is similar to the results obtained in Fig. 3. From Fig. 4 (a), the sound pressure level is enhanced by 25 dB on the center axis for the difference frequency at 100 Hz from δ=0 to δ=7. Similarly, a 15 dB enhancement is observed for the difference frequency at 200 Hz. However, the improvement of the directivity for low frequencies is not obvious even for δ=7. By increasing the difference frequency, the directivity can be improved under the same flare constant δ and a similar improvement on the directivity can be achieved at the same difference frequency by increasing the flare constant. For the difference frequency wave at 5000 Hz, the acoustic beam in the horned case (δ=7) mainly concentrates within $\pm 5^{\circ}$, which is greatly sharper than the non-horned case (δ=0) within $\pm 13^{\circ}$ as shown in Fig. 4(d). On the basis of these results, we found that a directive acoustic beam emitted from a PAL with specific difference frequencies is achieved, the beam directivity can be improved by using a horned PAL. It is also expected that an acoustic horn can be optimized by using the specific approach proposed to improve the efficiency [22].

On the improvement of horned emitters, the ratio of the equivalent radius (a_e) of a non-horned emitter to the radius (a_0) of a horned emitter for various horn lengths L_1 and flare constants δ is investigated in Fig. 5. Under a specific difference frequency, the ratio

a_e/a_0 increases with the horn length to indicate that a larger non-horned emitter should be used to reach the same directivity. For a larger flare constant, the ratio is even greater. If a horn has a length of 0.7 m and a flare constant is 5, the ratio is approximately equal to 5. It implies that the area of the non-horned emitter is 25 times with respect to that of the horned emitter. For a specific horn length, a greater flare constant will enlarge the radius ratio. Besides, the influence of the flare constant on the ratio becomes significant within the low-frequency range, see Fig. 5(b). The directivity effects of the horned PAL and the non-horned PAL under the same radius are also presented in the inserted graphs of Fig. 5. According to the present results, the function of acoustic horns to improve the directivity can be evidently demonstrated.

4. Conclusions

An analytical model for the difference frequency acoustic pressure generated by a horned PAL is proposed. For a specific case, i.e., an exponential horn, analytical solutions are obtained to investigate the performance of horned loudspeakers. From the obtained results, a horn can make a significant impact on the difference frequency acoustic pressure and the directivity effect generated by a PAL. The directivity can be further improved by increasing the flare constant at a specific frequency, and also the generated secondary sound pressure can be considerably enhanced by a horn in the low-frequency range. Besides, the radius of a non-horned emitter is found to be several times as large as that of a horned-emitter to reach a similar directivity. To compare with traditional types of PAL, an appropriate selection of the governing parameters can improve the performance of a horned PAL to produce highly directional acoustic waves. The present study offers an

analytical approach in engineering design of highly directional loudspeakers. In future works, a wide frequency bandwidth of directional acoustic waves in various potential applications will be explored.

Acknowledgements

The work described in this paper was supported by grants from the National Natural Science Foundation of China (Nos. 11702095 and 11702112), Natural Science Foundation of Jiangxi Province (No. 20171BAB216047) and Natural Science Foundation of Guangdong Province (No. 2016A030310090). Besides, the corresponding author (SK Lai) gratefully acknowledges the financial support provided from the Environment and Conservation Fund of the Government of the Hong Kong Special Administrative Region (Project No.: ECF Project 83/2017).

References

[1] Westervelt, P. J., 1963, "Parametric Acoustic Array," J Acoust Soc Am, 35(4), pp. 535-537.

[2] Ke, M. Z., Liu, Z. Y., Pang, P., Wang, W. G., Cheng, Z. G., Shi, J., Zhao, X. Z., and Wen, W. J., 2006, "Highly directional acoustic wave radiation based on asymmetrical two-dimensional phononic crystal resonant cavity," Appl Phys Lett, 88(26), 263505.

[3] Morvan, B., Tinel, A., Vasseur, J. O., Sainidou, R., Rembert, P., Hladky-Hennion, A. C., Swinteck, N., and Deymier, P. A., 2014, "Ultra-directional source of longitudinal acoustic waves based on a two-dimensional solid/solid phononic crystal," J Appl Phys, 116(21), 214901.

[4] Qiu, C. Y., and Liu, Z. Y., 2006, "Acoustic directional radiation and enhancement caused by band-edge states of two-dimensional phononic crystals," Appl Phys Lett, 89(6), 063106.

[5] Qiu, C. Y., Liu, Z. Y., Shi, J., and Chan, C. T., 2005, "Directional acoustic source based on the resonant cavity of two-dimensional phononic crystals," Appl Phys Lett, 86(22), 224105.

[6] Shi, C., and Kajikawa, Y., 2015, "A convolution model for computing the far-field directivity of a parametric loudspeaker array," J Acoust Soc Am, 137(2), pp. 777-784.

[7] Shi, C., and Kajikawa, Y., 2016, "Volterra model of the parametric array loudspeaker operating at ultrasonic frequencies," J Acoust Soc Am, 140(5), pp. 3643-3650.

[8] Cervenka, M., and Bednarik, M., 2013, "Non-paraxial model for a parametric acoustic array," J Acoust Soc Am, 134(2), pp. 933-938.

[9] Ding, D. S., 2000, "A simplified algorithm for the second-order sound fields," J Acoust Soc Am, 108(6), pp. 2759-2764.

[10] Ding, D. S., Shui, Y. G., Lin, J. B., and Zhang, D., 1996, "Simple calculation approach for the second harmonic sound field generated by an arbitrary axial-symmetric source," J Acoust Soc Am, 100(2), pp. 727-733.

[11] Gan, W. S., Yang, J., and Kamakura, T., 2012, "A review of parametric acoustic array in air," Appl Acoust, 73(12), pp. 1211-1219.

[12] Kamakura, T., Hamada, N., Aoki, K., and Kumamoto, Y., 1989, "Nonlinearly Generated Spectral Components in the Nearfield of a Directive Sound Source," J Acoust Soc Am, 85(6), pp. 2331-2337.

[13] Muir, T. G., and Willette, J. G., 1972, "Parametric Acoustic Transmitting Arrays," J Acoust Soc Am, 52(5), p. 1481.

[14] Yoneyama, M., Fujimoto, J., Kawamo, Y., and Sasabe, S., 1983, "The Audio Spotlight : an Application of NonLinear Interaction of Sound Waves to a New Type of Loudspeaker Design," J Acoust Soc Am, 73(5), pp. 1532-1536.

[15] Sayin, U., Artis, P., and Guasch, O., 2013, "Realization of an omnidirectional source of sound using parametric loudspeakers," J Acoust Soc Am, 134(3), pp. 1899-1907.

[16] Tanaka, N., and Tanaka, M., 2010, "Active noise control using a steerable parametric array loudspeaker," J Acoust Soc Am, 127(6), pp. 3526-3537.

[17] Shi, C., Kajikawa, Y., and Gan, W.-S., 2014, "An overview of directivity control methods of the parametric array loudspeaker," APSIPA Transactions on Signal and Information Processing, 3, p. e20.

[18] Sayin, U., and Guasch, O., 2013, "Directivity control and efficiency of parametric loudspeakers with horns," J Acoust Soc Am, 134(2), pp. El153-El157.

[19] Kinsler, L. E., 2000, Fundamentals of acoustics, Wiley.

[20] Hamilton, M. F., and Blackstock, D. T., 1998, Nonlinear Acoustics, Academic Press.

[21] Tang, K. T., 2007, Mathematical Methods for Engineers and Scientists 3: Fourier Analysis, Partial Differential Equations and Variational Methods, Springer.

[22] Farhadinia, B., 2012, "Structural optimization of an acoustic horn," Appl Math Model, 36(5), pp. 2017-2030.

Figure captions

Fig. 1 (a) (a) Schematic diagram of a horned parametric acoustic loudspeaker with a typical array of piezoelectric transducers; (b) and (c) configuration and coordinate system; and (d) a driven circuit of the parametric array.

Fig. 2 Comparison of directivity effect: (a) a non-horned PAL and a horned PAL with various flare constants (b) $\delta = 1$, (c) $\delta = 5$, and (d) $\delta = 7$.

Fig. 3 Variation of sound pressure levels for different flare constants. The amplitude of the primary frequency wave is $p_a = 10$ Pa. The inserted figure shows the acoustic pressure response in the low frequency range.

Fig. 4 Comparison of the sound beam directivity generated by a horned PAL and a non-horned PAL at various difference frequencies (a) 100 Hz, (b) 200 Hz, (c) 1000 Hz and (d) 5000 Hz. The amplitude of the primary frequency wave is $p_a = 10$ Pa.

Fig. 5 Ratio of the equivalent radius of a non-horned emitter to the radius of a horned emitter for (a) various horn lengths at 5000 Hz; and (b) various flare constants with a horn length of 0.5 m. The radius of the horned emitter is $a_0 = 0.1$ m for both (a) and (b). The inserted graphs show the directivity of the horned emitter and the non-horned emitter with $a_0 = 0.1$ m.

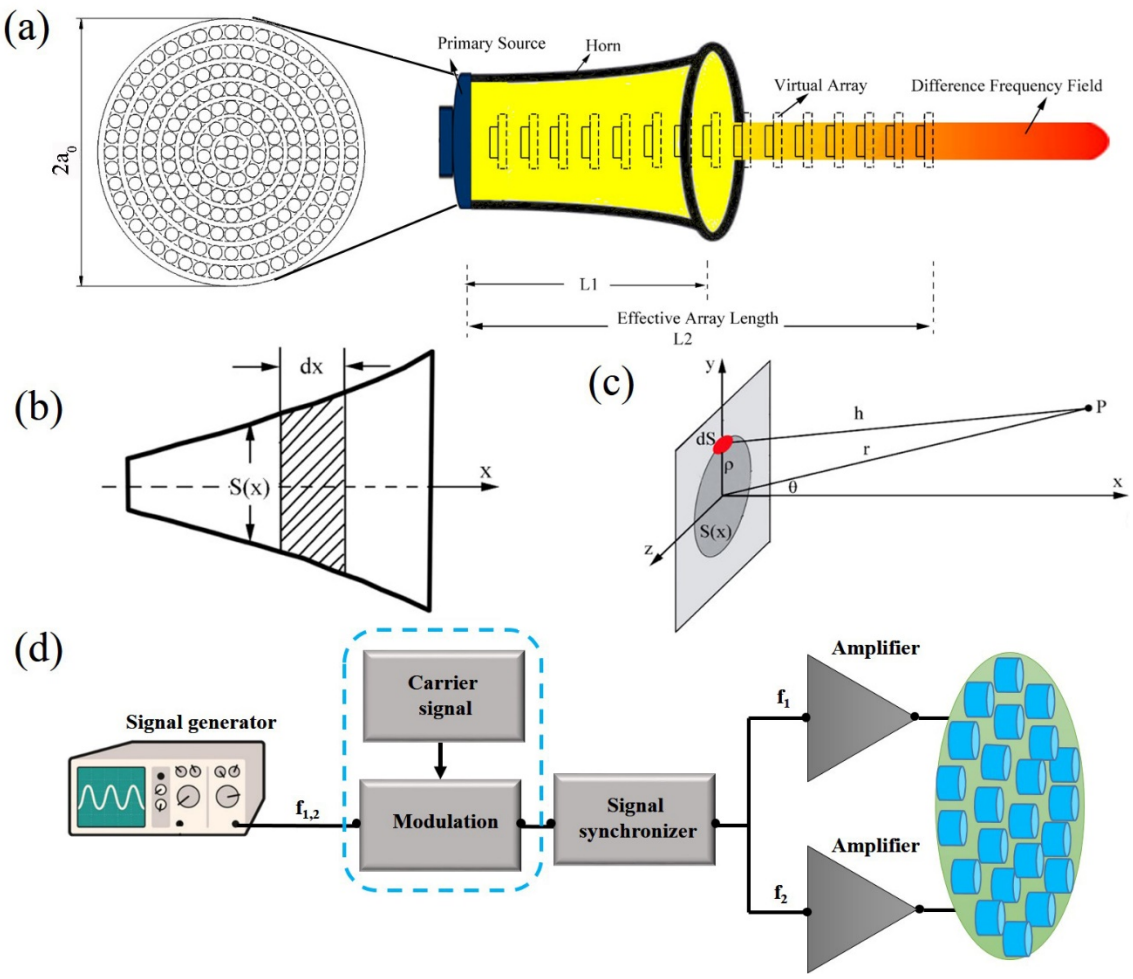

Fig. 1 (a) (a) Schematic diagram of a horned parametric acoustic loudspeaker with a typical array of piezoelectric transducers; (b) and (c) configuration and coordinate system; and (d) a driven circuit of the parametric array.

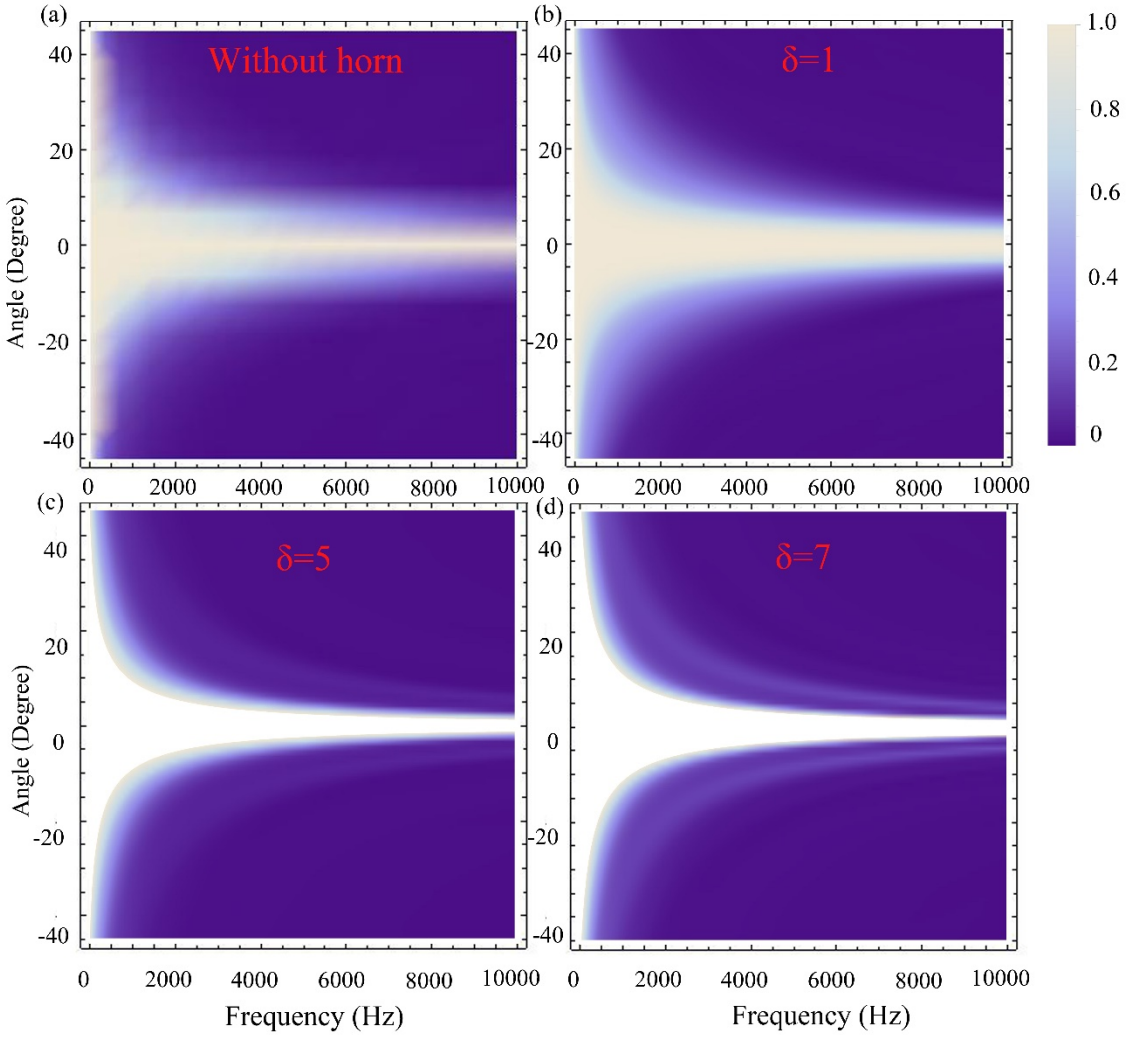

Fig. 2 Comparison of directivity effect: (a) a non-horned PAL and a horned PAL with various flare constants (b) $\delta = 1$, (c) $\delta = 5$, and (d) $\delta = 7$.

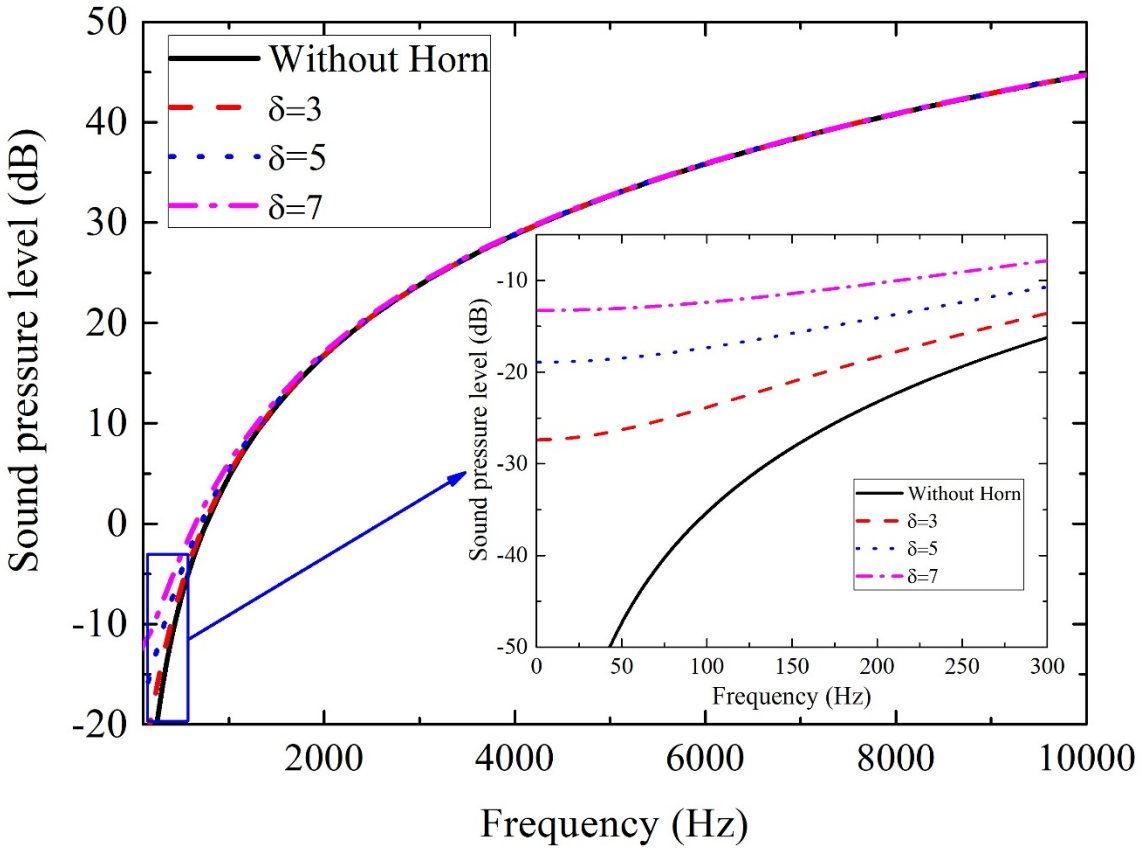

Fig. 3 Variation of sound pressure levels for different flare constants. The amplitude of the primary frequency wave is $p_a = 10$ Pa. The inserted figure shows the acoustic pressure response in the low frequency range.

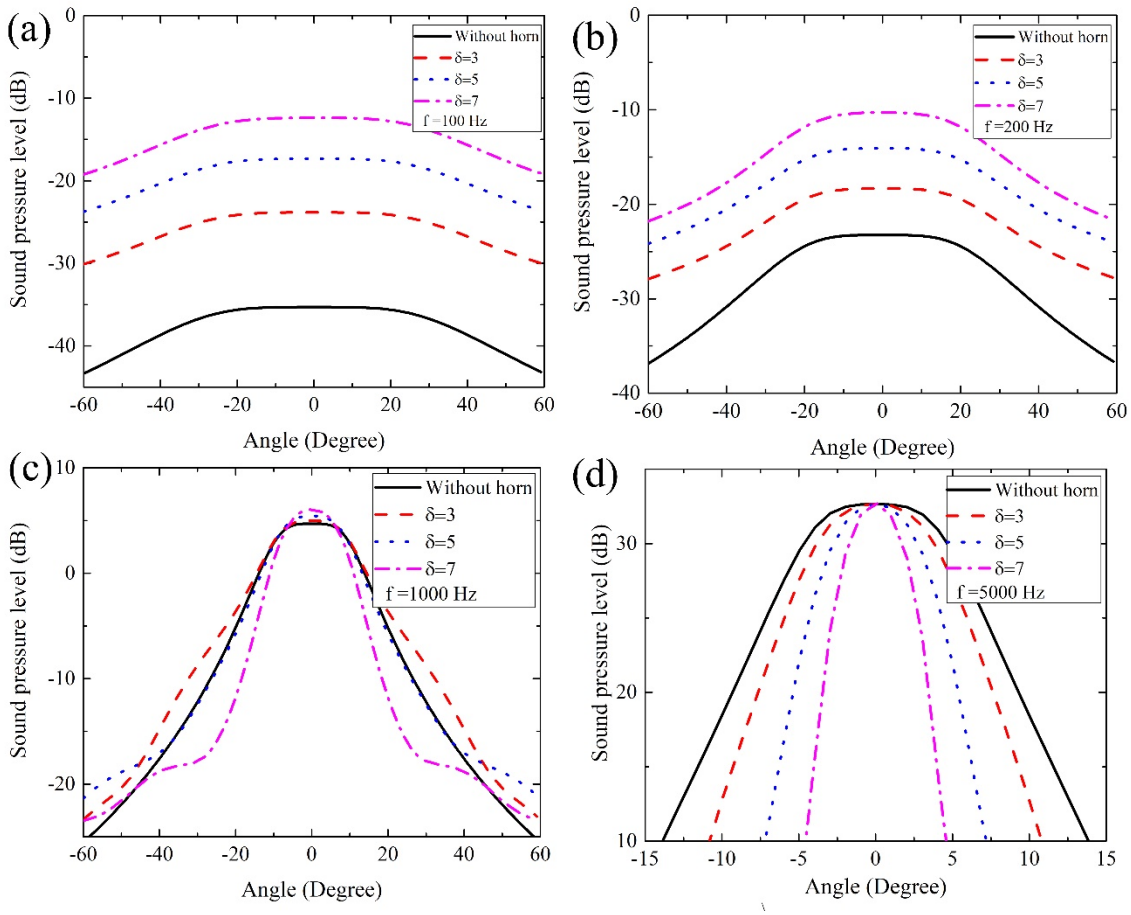

Fig. 4 Comparison of the sound beam directivity generated by a horned PAL and a non-horned PAL at various difference frequencies (a) 100 Hz, (b) 200 Hz, (c) 1000 Hz and (d) 5000 Hz. The amplitude of the primary frequency wave is $p_a = 10$ Pa.

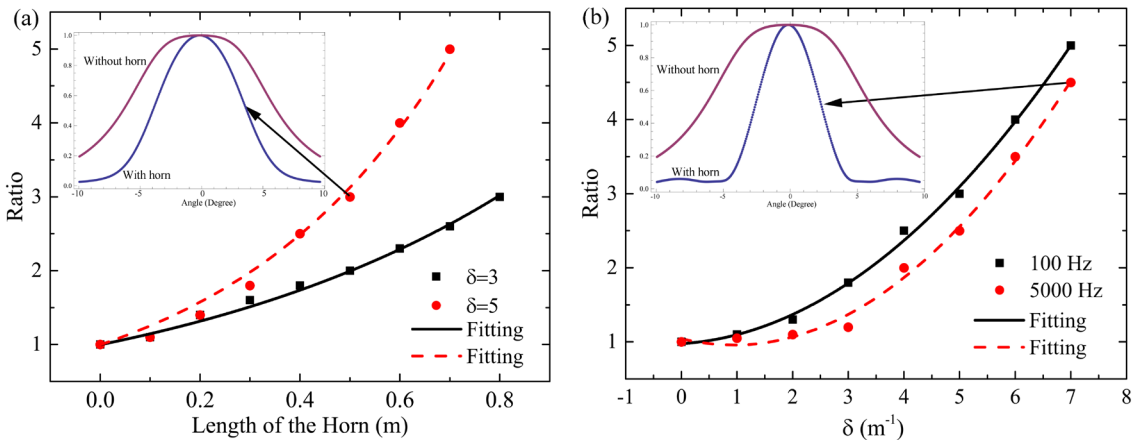

Fig. 5 Ratio of the equivalent radius of a non-horned emitter to the radius of a horned emitter for (a) various horn lengths at 5000 Hz; and (b) various flare constants with a horn length of 0.5 m. The radius of the horned emitter is $a_0 = 0.1$ m for both (a) and (b). The inserted graphs show the directivity of the horned emitter and the non-horned emitter with $a_0 = 0.1$ m.